Journal of Engineering Science and Technology
Vol. 15, No. 5 (2020) 3281 - 3302

INTEGRATED ANALYSIS OF MOTIONS AND LOADS RESPONSES OF A WAVE-PIERCING TRIMARAN IN WAVES

A. ASKARIAN KHOOB[1], M. J. KETABDARI[1,*]

[1]Department of Marine Technology, Amirkabir University of Technology,
Hafez Ave, No. 424, P.O. Box 15875-4413, Tehran, Iran
*Corresponding Author: ketabdar@aut.ac.ir

Abstract

Trimaran is a multihull vessel that consists of a long slender center hull with two small outriggers or side hulls that are connected to the main hull by a cross structure. Hydrodynamic interactions between the main and side hulls cause significant loads applied to the transverse structure. This paper investigates the numerical analysis of the wave-induced motions and loads of a wave-piercing trimaran traveling in waves. A global finite element model of the ship integrating structural and hydrodynamic analysis was built with the MAESTRO software. The numerical estimation was carried out using an advanced computer program based on the 3D panel potential theory called MAESTRO –Wave. The MAESTRO-Wave takes advantage of the existing structural mesh and defined loads to formulate the equations of motion. This approach results in a perfectly balanced structural model without using "inertia relief." The investigations demonstrated that interactions between the motions with the wave-induced loads and individual motion responses together, lead to the frequent appearance of "kinks" in a coupled form with the responses of other motions or wave-induced loads. The results also showed that the motion and the wave-induced load responses in the beam seas were found to be insensitive to the effects of the changes in the vessel speeds.

Keywords: Cross deck, Frequency domain computation, Trimaran model, Ship motions, Wave-induced loads.

1. Introduction

In recent years the demand for high-speed multihull ships for military, commercial, and recreational applications has been significantly increased. The trimaran is a multihull thin vessel that consists of three independent hulls, a long main hull and two slim side hulls (outriggers). Because of high hydrodynamic and operational performance, trimaran ships have been of interest to naval architects, especially in research, ferry and military applications. Compared with conventional monohull and other high-speed crafts, this advanced ship possesses many merits including [1, 2]:

- Less power and excellent fuel consumption efficiency because of low wave resistance at high speed.
- Remarkable speed, agility and quick accelerating performance due to slender hull form.
- Improved seaworthiness and seakeeping quality due to less transverse stiffness and high damping of the roll.
- Perfect transverse stability without being too stiff due to the suitable alignment of lateral hulls.
- Flexible layout and superior general arrangement because of large deck space and wide overall beam.
- Strong survivability and improved damage stability because of extra protection provided by the side hulls.

In contrast to traditional monohull ships, trimaran will experience new cases of wave loads when advancing at sea because of its unique configuration and existence of cross structure. The fluid force acting on the outrigger of the trimaran vessel will be transfer to the main hull by cross structure. Then a trimaran is subjected to transverse wave loads. Prediction of wave-induced motion and load of a trimaran is very important in the preliminary structural design. Many researchers have studied resistance characteristics of the trimaran, but little research has been conducted on wave-induced motion and load of the trimaran.

Fang and Too [3] predicted the effect of the side hull location on the motions of a trimaran using the 3D pulsating source distribution method. They showed that the trimaran ship design with larger clearance and smaller stagger is generally advantageous from the wave motions viewpoint. Armstrong [4] presented trials and measurements conducted on Benchijigua Express trimaran fast ferry. In their research, improved pitch and roll characteristics were presented and generally improved levels of comfort were compared with the catamaran. Their results demonstrated a 50% reduction in passenger seasickness for the trimaran. Sato et al. [5, 6] developed a WISDAM-XI code for the prediction of the motion performance of a trimaran vessel. They validated the code accuracy through the comparison with experimental data. They showed that in the case of heave and pitch motions predicted values had reasonable accuracy while the roll motion amplitude was slightly overestimated. WISDAM-X and WISDAM-XI are two versions of the CFD ship-motion simulation codes. The WISDAM-X code is particularly used for the design of conventional type ships while WISDAM-XI code is used for the prediction of hydrodynamic performance of multi-hull vessels. In the WISDAM-X method, RANS and continuity equations are solved on the overlapping grid system using finite-volume discretization. WISDAM-XI

method is modified into a multi-block grid system in order to cope with the complicated configuration of a multi-hull vessel.

Hebblewhite et al. [7] investigated the effects of the stagger of the side hulls on the motions in heave and pitch of a representative trimaran hull. They conducted experimental investigations for four different longitudinal (stagger) positions of the side hull. Longitudinal shifts of the outriggers towards the aft increased the pitch radius of gyration. Their investigations demonstrated that this variation and the resulting variation in the pitch radius of gyration could have a significant effect on the heave and pitch motions. Fang and Chen [2] conducted a spectral analysis based on the wave-induced loads to select suitable side hull location for a trimaran ship advancing in waves. They applied the 3D source distribution method, using a combination of pulsating source potential and the panel method, to drive wave load with respect to different staggers and clearances. Min and Shi-lian [8] calculated significant values for wave loads of a trimaran with different layouts and lengths of the side hulls based on 3D potential theory and Green's function.

Mohammadi et al. [9] calculated the global loads acting on a trimaran in intact and damaged conditions. They used the strip theory and panel method to predict still water static and wave-induced dynamic loads in the frequency domain. The analysis carried out using ShipX (VERES) and MAESTRO-Wave codes. A comparison of the results shows a good agreement between the results of the two numerical solutions. Vakilabadi et al. [10] studied heave and pitch motions of a trimaran vessel at different Froude numbers in a towing tank. They showed that increasing the Froude number leads to rapidly descending post-resonance-peak regions of the heave Response Amplitude Operator (RAO) diagrams. They also showed that the sensitivity of pitch RAO on the changes in the values of Froude number and wave amplitude is not so great when the non-dimensional wavelength is less than 0.8. Also, for the non-dimensional wave frequency values greater than 2.5 to 2.8, the pitch RAO does not experience any significant changes as a result of variations in the Froude number or wave amplitude. Pei et al. [11] predicted the long-term prediction on the wave load of a flat-type river-sea-going container ship. Probability analysis theory for wave loads consists of two steps, short-term and long-term prediction. Short-term prediction predicts for a short period, e.g. half an hour to three hours, when the significant wave height and the average wave period are considered constant. Long-term prediction means to statistically predict the reaction of a ship to irregular waves over a long period, with duration of 20 to 25 years. The long-term distribution and its probability density function in irregular waves can be fitted by overlying the short-term values according to their appearance probability illustrated in wave scatter diagrams [12].

The Linear Elastic Compass Wave Loads Calculation System (WALCS-LE) which is a numerical linear hydro elastic investigation and is used in the study of wave-induced motion and load responses of a 400,000 deadweight tonnage (DWT) was utilized by Adenya et al. [13]. The long-term prediction results provide valuable insights into the extreme response values that a ship experience in its lifetime [10]. MAESTRO-wave was also used by Prini et al. [14] to examine the sea-keeping performance of a search and rescue craft (lifeboat) in regular waves. The validity of the numerical model was verified through a broad comparison between the experimental model tests and the full-scale trials. Xiaobo et al. [15], by performing numerical computations using WACLS and WASIM software, performed a series of experiments on a segmented model of a trimaran in different

sea conditions. The comparison made between measured results of zero speed and non-zero speed matched better with the numerical computation of zero speed. An experimental methodology with a large-scale segmented was performed by Jiao et al. [16]. The experimental data were compared with a numerical analysis of the short-term prediction that was made using an in-house code. The predicted values agreed with experimental measurements. Khoob and Ketabdari [17] investigated the influence of side hulls configuration (symmetric, inboard and outboard types) for wave loads on cross-deck of a wave-piercing trimaran. The computation of these hydrodynamic forces is carried out using the MAESTRO-Wave 3D panel method code. The results demonstrate that the outboard side hull form has the best performance on wave-induced load among three kinds of side hull forms.

In this research 3D panel method code of MAESTRO-Wave was used to analyse the wave-induced motion and load of a wave-piercing trimaran. The study offers useful information about wave loads for balancing seakeeping performance with other design considerations in the conceptual design of a wave-piercing trimaran.

2. The hull form and principal dimensions

Designing trimaran faces many technical challenges because of its special hull configuration and higher operational speeds. Therefore, in comparison with mono-hull ships, more design parameters should be considered in both hydrodynamic and structural points of view. In this work, a trimaran was initially designed based on the prescription of the American Bureau of Shipping rules (ABS) [18] for high-speed naval crafts. Moreover, the reports on designing models of trimaran ship, including RV Triton, LCS-2 independence; Bechijiqua Express and Austal 102 were employed in the present study [19].

A global Finite Element (FE) model of a trimaran was built in the full load condition using the MAESTRO program [20]. The model is composed of the main hull, two side hulls, and two cross deck structure joining the three hulls together. A wave-piercing bow was used to improve the hydrodynamic performance of the ship. The main tanks and compartments were situated in both central and side hulls of the model. The superstructure is not modelled, but this part and main ship components and payloads (including basic machinery, generators, weapon systems with ammunition and helicopters) were modelled as concentrated weights distributed on a certain number of nodes. The FE model was created using five sub structural units with 28 modules, 5941 nodes and 13090 elements which collectively formed the model of the ship.

The structural components include strake panels, frames, beams, columns, and plate elements. Modeling the FE of trimaran was performed in the MAESTRO software using CQuadR Stiffened Panel, CTRIR Triangle Element, Crowd and Compound elements. The marine steel grade of AH36 was used as the structural material for the model to achieve lower building cost and fatigue. Main ship components and payloads (deckhouse, basic machinery, generators, weapon systems with ammunition and helicopters) were modelled as weights, which are distributed on a certain number of nodes. The structural configuration of the model for the main hull, outriggers and cross decks is a longitudinal framing system with frame spaces of 1000 mm. Special considerations were taken into account at the junctions of cross decks and the main hull to avoid stress concentration on the main hull. According to the ABS rules, minimum scantlings were defined for each

member. The strength of the midship section was controlled for global and local design loads. The FE model is shown in Fig. 1. Principal dimensions of the trimaran model are reported in Table 1.

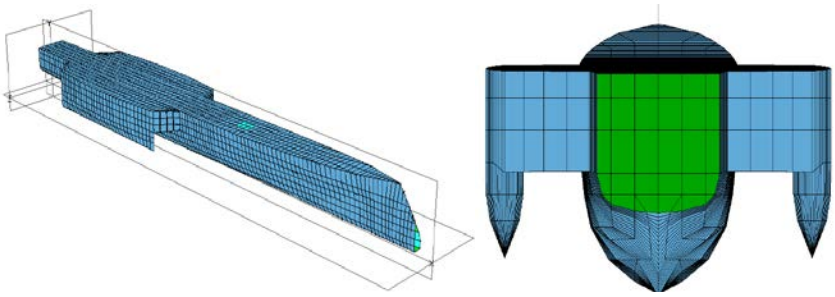

Fig. 1. A global FE model of the trimaran.

Table 1. Main parameters of the trimaran.

Item	Value
Length overall [m]	121
Length on waterline [m]	120.2
Beam overall [m]	24.17
Beam on waterline [m]	10.66
Depth [m]	13.03
Draught [m]	4.86
Length of the side hull [m]	40
The beam of the side hull [m]	2.62
Depth of the side hull [m]	9.04
Draft of the side hull [m]	2.84
Clearance between the centreline of the main hull and the centreline of the side hull [m]	10.77
Stagger between the mid-ship of side hull and the mid-ship of the main hull [m]	25.41
Displacement [ton]	2435.93
Design speed [Knot]	30

3. Methods

A 3D panel linear code called MAESTRO–Wave was used to predict the wave loads of this vessel. This program uses the Green's function integral equation's technique to determine the unsteady potentials to solve the boundary value problem of interaction between water waves and bodies in the frequency domain. Imagine that a ship advances at a steady speed U while the amplitudes of its motions and incidental waves are small and the fluid is homogeneous and incompressible. The overall velocity potential in the fluid domain can be separated into two parts [20]:

The RAO (response amplitude operator) can be obtained by solving the linear equation of motion. In order to solve this equation the values of mass matrix, added

mass, damping coefficient, the restoring coefficient and exciting force and moment have to be calculated first. Imagine that a trimaran ship advances at a steady speed U while the amplitudes of its motions and incidental waves are small and the fluid is homogeneous and incompressible. The total velocity potential $\Phi(x,y,z)$ in the fluid domain can be expressed as:

$$\Phi(x,y,z)_{Total} = [-Ux + \varphi(x,y,z)]_{\text{Double Body}} + \left[\left(\phi_I + \phi_D + \sum_{j=1}^{6} \eta_j \phi_j\right) e^{i\omega_e t}\right]_{unsteady} \quad (1)$$

where η_j are the motion amplitudes of six modes. The incident wave potential in this equation is known for a sinusoidal wave and is defined as follows:

$$\phi_I = i\frac{g\alpha}{\omega} e^{-ik(xcos\beta - ysin\beta)}\, e^{kz} \quad (2)$$

where α is the wave amplitude, ω_e is the encountered wave frequency, which is due to the ship speed U, $k = \omega^2/g$ is the wave number, β is the wave heading angle (β =0 for the following wave) and ω is the wave frequency (Fig. 2).

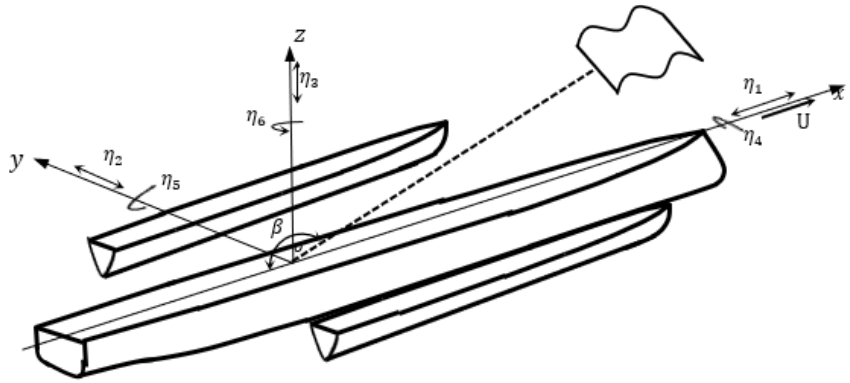

Fig. 2. The coordinate system of the trimaran ship.

where ω_e is defined as follows:

$$\omega_e = |\omega - Ucos\beta| \quad (3)$$

Based on potential flow theory, all the individual potentials must satisfy the linear boundary conditions and the Laplace equation in the fluid domain as well as the appropriate radiation conditions at infinity. After obtaining the velocity potentials, the pressure which acts on the hull of the craft as a result of the given wave conditions can be calculated from the linearized Bernoulli's equation which is expressed as:

$$p = -\rho\left(\frac{\partial \Phi}{\partial t} + \frac{1}{2}|\nabla\Phi|^2 + gz\right) \quad (4)$$

In order to predict the wave induced loads and motions of the ship, the equation of coupled linear motions is written as follows:

$$\sum_{k=1}^{6}\left[-\omega_e{}^2\left(M_{jk}+A_{jk}\right)+i\omega_e B_{jk}+C_{jk}\right]\eta_k = X_j \qquad ,k=1,2,\ldots,6 \tag{5}$$

where M_{ij} is the mass matrix, A_{jk} and B_{jk} are the added mass and damping coefficient which originate from the radiation potential. X_j is the exciting force due to the incident and diffracted wave potential.

The RAO η_k can be obtained by solving the complex coefficient linear equation. The wave-induced bending moment (BM) and shear force (SF) in the wave are defined as:

$$\begin{bmatrix} Q_x \\ Q_y \\ Q_z \\ M_x \\ M_y \\ M_z \end{bmatrix} = \iint_B p \begin{bmatrix} n_1 \\ n_2 \\ n_3 \\ n_4 \\ n_5 \\ n_6 \end{bmatrix} ds - \omega_e^2 [M] \begin{bmatrix} \eta_1 \\ \eta_2 \\ \eta_3 \\ \eta_4 \\ \eta_5 \\ \eta_6 \end{bmatrix} \tag{6}$$

The definition of the wave-induced forces and moments acting on the cross deck are shown in Fig. 3. These forces and moments include: Longitudinal in-plane Force (Q_X), transverse vertical shear forces (Q_Y), Transverse in-plane Horizontal Force or Side Force (Q_Z) , Transverse vertical bending moments or roll moment (M_X), horizontal in-plane moments or yaw moment (M_Y) and transverse torsional moment or pitch moment (M_Z). M_X, M_Z and Q_Y are very important for cross structure analysis.

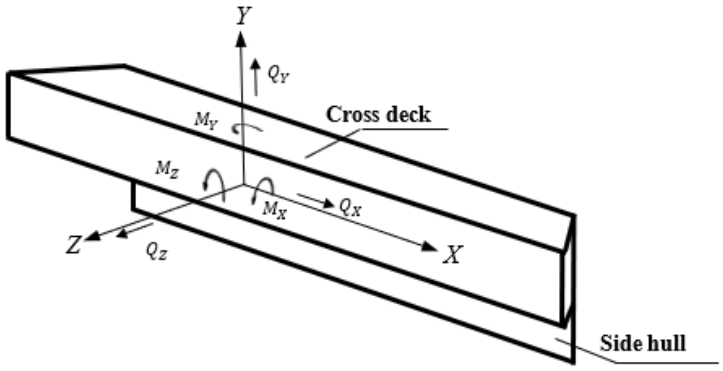

Fig. 3. Representation of the wave-induced forces and moments acting on cross deck.

4. MAESTRO-Wave computational verification

MAESTRO software is a naval architecture based design tool that seamlessly integrates hydrodynamics, FE analysis, limit state failure mode evaluation, ultimate hull girder analysis, structural optimization, extreme load analysis and spectral fatigue analysis under a single user interface. This is a commercial powerful ship design, analysis and evaluation program that is currently used by the navies,

classification societies, design offices and universities. The MAESTRO-Wave is an integrated frequency-domain/time-domain computational tool to predict the motions and wave loads of floating structures.

The code has been developed based on the potential flow theory using the 3D panel method. The main attraction for using this software is that it does not require the use of Finite Element (FE) mesh separate from the hydrodynamic mesh when performing the structural analysis of the same hull geometry. This process, therefore, ensures that there is equilibrium between the hydrodynamic and the FE mesh; hence it reduces the difficulty of convergence between the two different meshes which is commonly experienced when importing the hydrodynamic mesh into an FE program. The equations of motion are formulated using the structural mesh rather than the hydrodynamic mesh. This approach results in perfect equilibrium for the structural model. Bending moments, shear forces and torsional moments are automatically enclosure. No inertia relief and artificial loads are needed to balance the model [20].

The S-175 container ship is a well-known standard test case because it was used by the ITTC [21] to carry out a comparative numerical study of linear wave-induced structural loads and motions. The database that resulted from that study includes some experimental data and also numerical results from many institutions. In order to validate the theoretical capacity of MAESTRO -wave to predict the motion characteristics of ship hull forms over a range of wave frequencies and Froude numbers, a comparison was conducted with the available experimental data of S-175 [22]. MAESTRO-Wave seakeeping model of S-175 is shown in Fig. 4.

The motion RAO results and wave-induced loads, along with the available experimental data from ITTC, are shown in Figs. 5 to 8. All results are presented in a non-dimensional way using wave amplitude (A), wavenumber (k), encounter frequency (ω), water density (ρ), gravitational acceleration (g), ship beam (B) and ship length between perpendiculars (Lpp) as given in Table 2. The comparison shows that this method has acceptable accuracy for predicting wave-induced loads and motion of the ship.

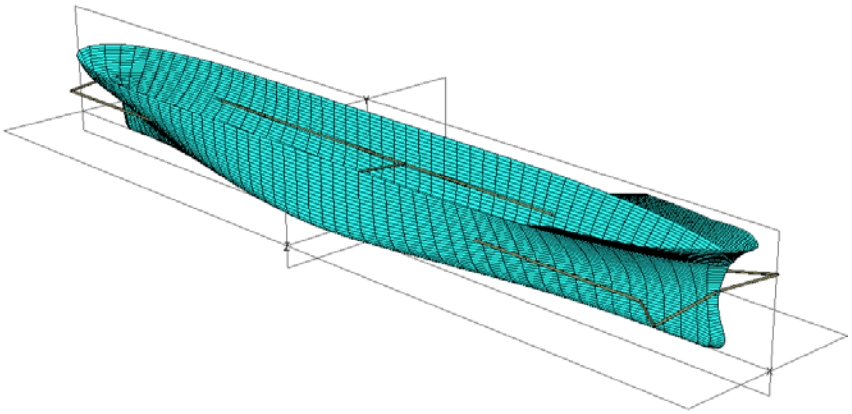

Fig. 4. MAESTRO-Wave seakeeping model of S-175 container ship.

Table 2. Main parameters of the S-175.

Item	Value
The length between perpendiculars [m]	175
Beam [m]	25.4
Depth [m]	15.4
Draft [m]	9.5
LCG aft of midship [m]	2.5
XG(from AP) [m]	84.97
The vertical center of gravity[m]	9.55
YG (from centreline) [m]	0
Block coefficient	0.572
Midship section coefficient	0.98
Displacement [ton]	24742
Design speed [Knot]	22.145

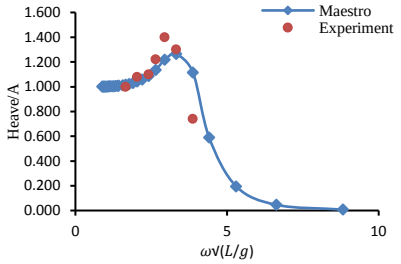

Fig. 5. RAOs of heave motion in beam seas at $F_n = 0.275$.

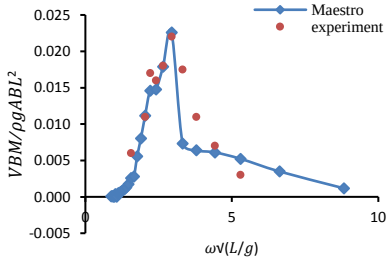

Fig. 6. RAOs of vertical bending moments in head seas at $F_n = 0.275$.

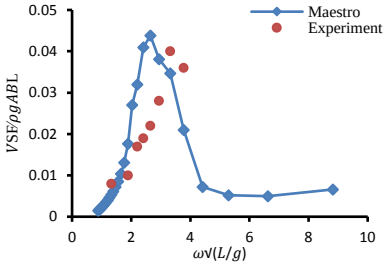

Fig. 7. RAOs of Vertical shear forces in bow quartering seas ($\beta = 150$) at $F_n = 0.275$.

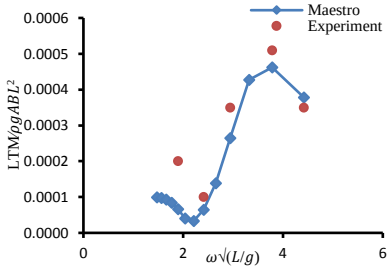

Fig. 8. RAOs of Longitudinal torsion moments in bow quartering seas ($\beta = 150$) at $F_n = 0.275$.

5. Results and discussions

The purpose of this study was to the prediction of motions and wave loads responses of a wave-piercing trimaran in regular waves. Three different speeds and wave headings are used to predict motion and hydrodynamic loads. The speeds were 10 knots, 20 knots and 30 knots. The wave headings were beam seas (90^0), bow quartering seas (135^0) and head seas (180^0) that are usually of greatest concern in the seakeeping design. The seakeeping analysis was performed to compute the wave loads for wave periods in the range of 3 to 30 sec at increments of 1 sec. This corresponds to wave frequencies range of 0.21 to 2.1 rad/s with an increment of about 0.068 rad/s associated with 28 data in this range.

RAOs of wave load and motion can be viewed graphically in the MAESTRO in all sections or a specific section of the ship. Users can select the node at the maximum value and recover the location, condition and maximum value. In order to study the wave loads on a trimaran, the node at the maximum value is used to evaluate the vertical bending moment and vertical shear force. To investigate the transverse bending moment the section which connects the cross structure and the main hull was selected. This study presents RAO of wave responses in the frequency-domain mode. Weight and buoyancy distributions are shown in Figs. 9 and 10. A characteristic carpet plot of bottom pressure distribution in the head wave at 30 knots for wavelength 126.2 m with a unit amplitude shown in Figs. 11 and 12.

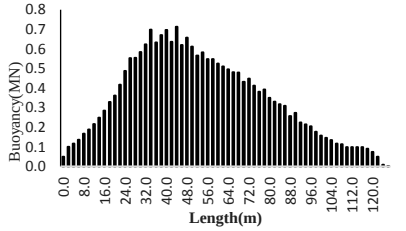

Fig. 9. Buoyancy distribution in full load condition.

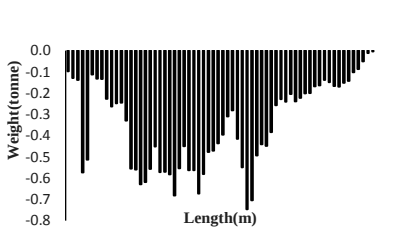

Fig. 10. Gross weight distribution in full load condition.

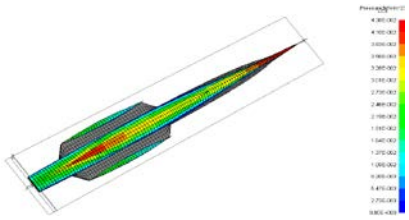

Fig. 11. Wave pressure distribution for Sagging condition (blue minimum, red maximum).

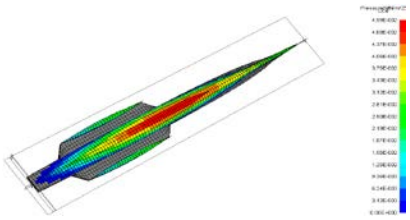

Fig. 12. Wave pressure distribution for Hogging condition (blue minimum, red maximum).

5.1. Wave motions

Figures 13 to 15 present the heave motion RAOs at different speeds. As shown in Fig. 13, heave responses for beam seas are almost the same for all three different speeds as expected since the speed does not affect the responses in the Beams Seas conditions. It is observed that response is almost constant for frequencies less than 1rad/s and after this frequency decreases linearly.

Figure 14 shows RAOs in bow quartering seas. It can be seen that the responses are nonlinear with respect to the wave frequencies and the plots also contained a "kink" smaller than unity. The "Kink" is due to the coupling of the heave and pitch

motion responses at their respective frequencies. These changes in the vessel speeds affect the peak magnitude response of the models in this heading. There is a clear distinction between their magnitudes at a vessel speed of 30 knots that has a peak of greater than unity. This occurs close to the trimaran ship's natural period. The peak is due to resonance. Trends of results in the head seas shown in Fig. 15 are nonlinear with respect to the wave frequencies. It is perceived that trend of heave motion responses in head seas is similar to the bow quartering seas but has greater magnitudes in "Kinks".

In summary, heave responses are not sensitive to changes in the vessel speeds in beam seas. Figures 13 to 15 represent that the RAOs tend to unity at low frequencies. At very low frequencies, the wavelength is large when compared with the trimaran dimensions; this is where the trimaran simply moves up and down with the wave and behaves like a cork. At high frequencies, the response tends to zero since the effect of very short waves cancel out over the length of the trimaran. For an RAO value of greater than unity, the trimaran response is greater than the wave amplitude (or slope).

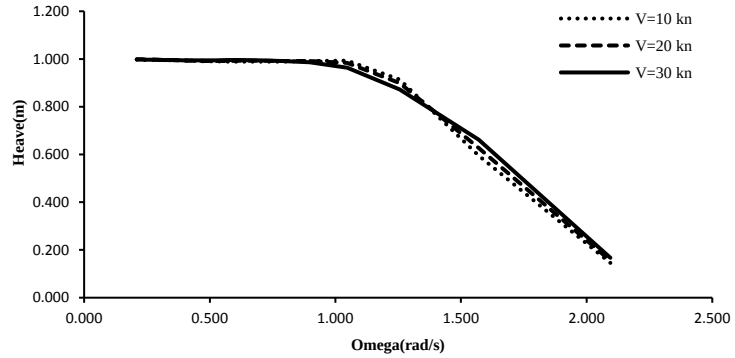

Fig. 13. RAOs of heave motions in Beam seas.

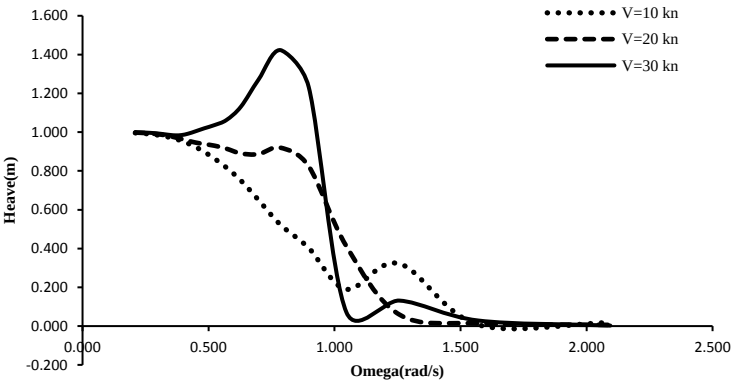

Fig. 14. RAOs of heave motions in Bow quartering seas.

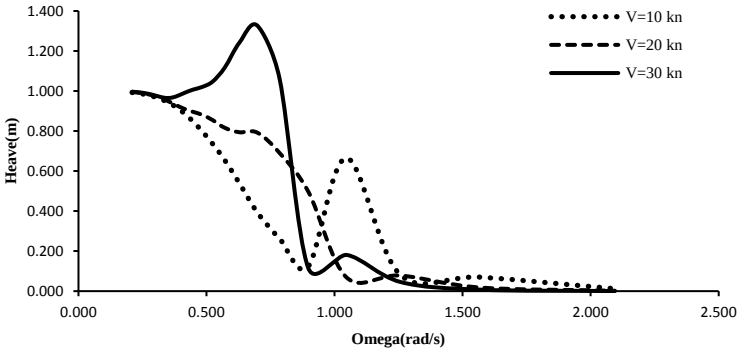

Fig. 15. RAOs of heave motions in head seas.

The RAOs of pitch motions are presented in Figs. 16 to 18. Figure 16 shows RAOs in beam seas. The pitch RAO shows the same trend for different vessel speeds within the range of wave frequencies. The magnitudes increase as the frequency increases but they demonstrate an inverse relationship between the increase in the vessel speeds and the magnitudes of the response at frequencies ranging from 1 to 1.5 rad/s. Above 1.5 rad/s, the higher the vessel speed the higher the response. Nevertheless, the magnitude of the peak response does not seem to be affected by the vessel speed. Figure 17 shows RAOs in bow quartering seas. It can be seen that the response is slightly linear with respect to the wave frequencies. This happens in all the vessel speeds between a frequency range of 0.21 to 0.57 rad/s. However, they then gradually demonstrate a nonlinear behaviour with respect to the wave frequencies at higher frequencies. In proceeding responses due to the individual vessel, speeds are detached from each other. The magnitudes of the responses to peak points also increase with an increase in the vessel speed. The pitch motion response in the head seas is illustrated in Fig. 18. It is seen that responses are closely similar to quartering seas.

In summary in beam seas, the magnitudes of the peak responses are not sensitive to changes in the vessel speed. It is also evident that the responses of pitch motion are closely similar to the head and bow quartering seas.

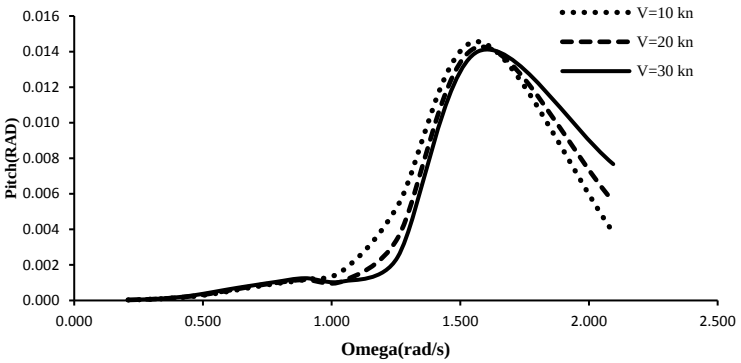

Fig. 16. RAOs of pitch motions at Beam seas.

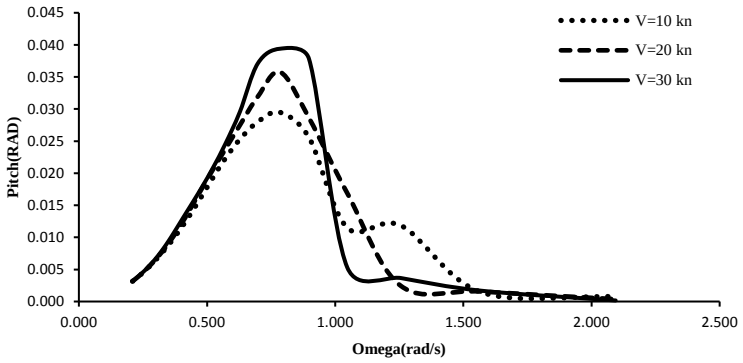

Fig. 17. RAOs of pitch motions at Bow quartering seas.

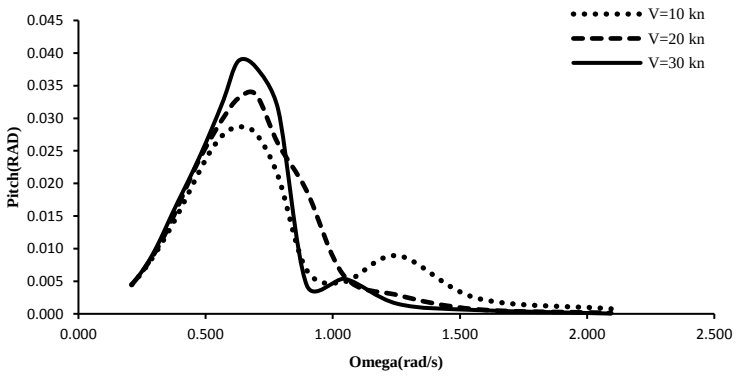

Fig. 18. RAOs of pitch motions at Head seas.

5.2. Longitudinal wave loads

Figures 19 to 21 present vertical bending moments RAOs at different speeds. Figure 19 shows RAOs in beam seas. It can be seen the responses at frequencies ranging from 0.21 to 0.7 rad/s and above 1.57 rad/s are approximately the same for all three speeds of the vessel. Within the frequency range 0.7–1.5 rad/s a higher speed also generates a higher response. Figure 20 shows RAOs in bow quartering seas. It can be seen that the response is slightly linear with respect to the wave frequencies and the same in the entire vessel speeds between a frequency range of 0.37 to 0.70 rad/s. This response then became nonlinear throughout the remainder of the frequencies and due to the individual vessel speeds, they are detached from each other. The responses contain two obvious high magnitudes "Kinks" with a magnitude less than the peak magnitude at a vessel speed of 30 knots and one "Kink" for other speeds at a higher frequency. The peak magnitudes of the three speeds are approximately the same. Figure 21 shows RAOs in head seas. It is observed that the vertical bending moment's responses are different for different speeds. The trend of the responses is nonlinear and contains a kink for vessel speeds of 20 and 30 knots. The "kinks" reveal the coupling of the pitch response and the vertical bending moment response in head and bow quartering seas.

The RAOs of vertical shear forces are presented in Figs. 22 to 24. Figure 22 shows RAOs in beam seas. It can be seen the responses at frequencies ranging from 0.21 to 0.7 rad/s and above 1.8 rad/s are approximately the same for all three speeds of the vessel. Within the frequency range 0.7–1.8 rad/s a higher speed also generates a higher response. Figure 23 shows vertical shear forces RAOs in bow quartering seas. Responses are linear with respect to the wave frequencies between a frequency range of 0.50 to 0.90 rad/s. Then vertical shear force differs for various speeds while they also contain a few "Kinks". These "Kinks" are due to the coupling of the pitch motions with the responses of the vertical shear force.

These changes in the vessel speeds affect the responses at higher frequencies in this heading. There is a clear distinction between their peak magnitudes at a vessel speed of 30 knots which has the highest responses. The vertical shear force response in the head seas is illustrated in Fig. 24. It is perceived that vertical shear forces are nonlinear with respect to the wave frequencies and contains some "Kinks" within the frequency range 0.5–1 rad/s. So, vessel speeds influence the trend and peak values. The response has the highest peak value at a vessel speed of 30 knots.

In summary, the peak values of vertical shear forces increase as the vessel speed increases. Also, the plots contain some "Kinks" whose numbers and magnitudes increase as the vessel speed increases.

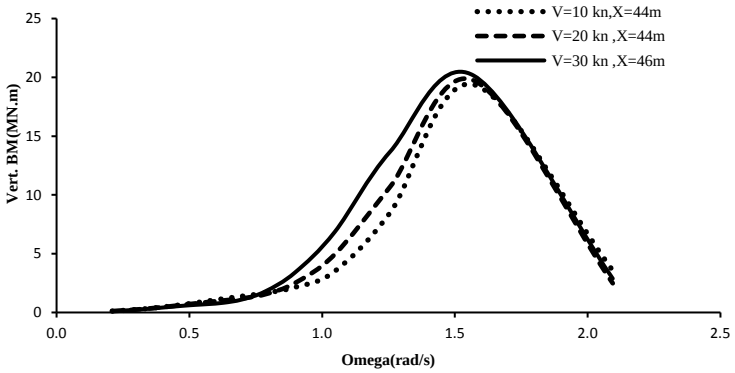

Fig. 19. RAOs of vertical bending moments at beam seas.

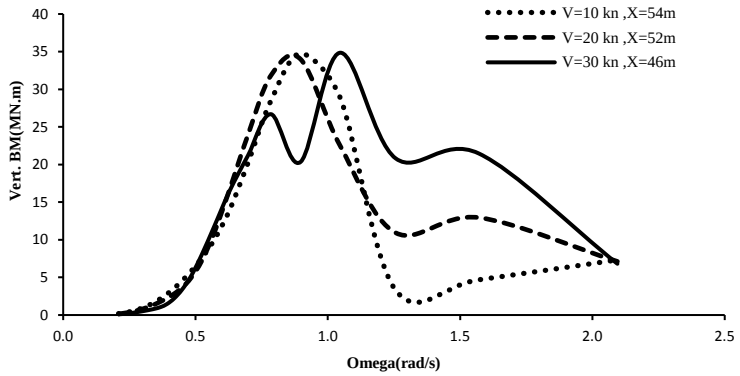

Fig. 20. RAOs of vertical bending moments at bow quartering seas.

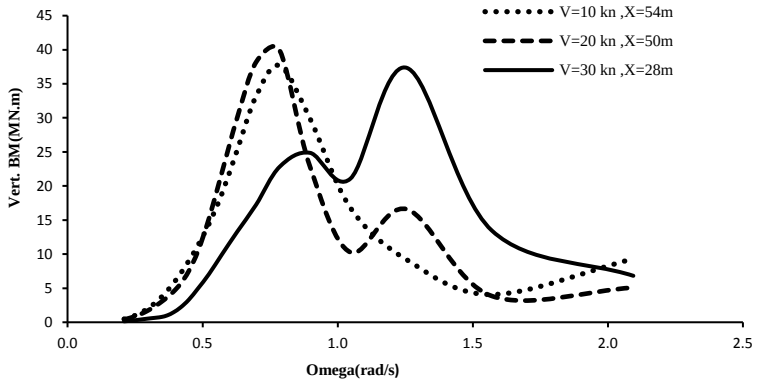

Fig. 21. RAOs of vertical bending moments at head seas.

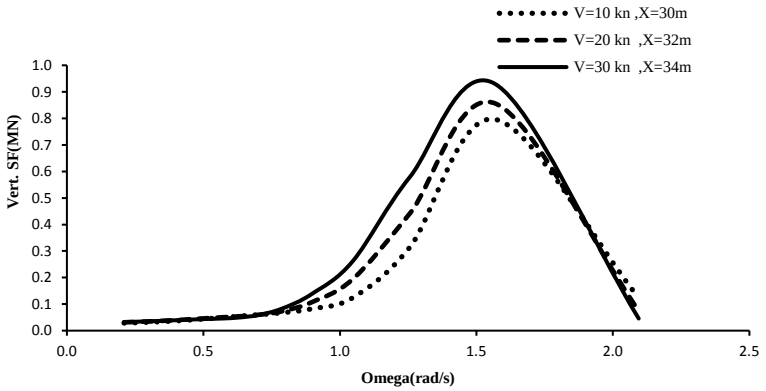

Fig. 22. RAOs of vertical shear forces at beam seas.

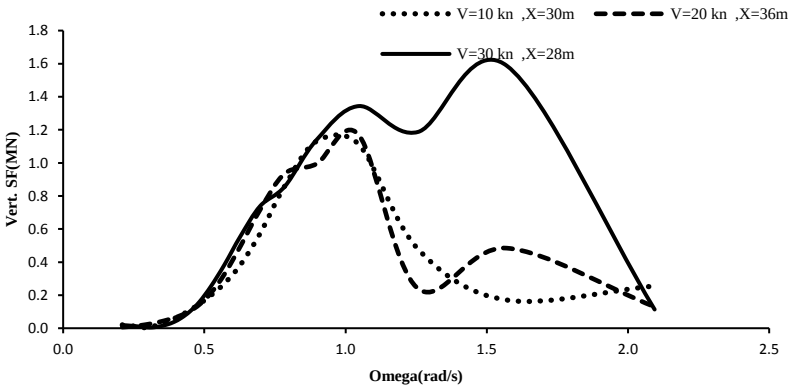

Fig. 23. RAOs of vertical shear forces at bow quartering seas.

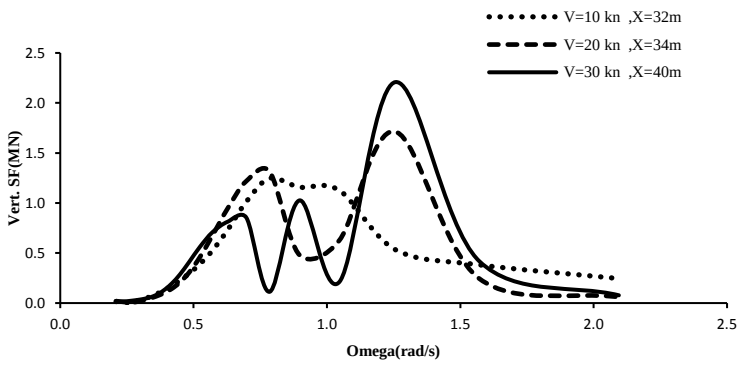

Fig. 24. RAOs of vertical shear forces at head seas.

5.3. Transverse wave loads

The RAOs of transverse bending moments are presented in Figs. 25 to 27. The transverse bending moment's response in the beam seas is shown in Fig. 25. The responses are nonlinear throughout the frequencies. The plots are similar in magnitude and physical trends to the responses except for maximum points for the beam seas. The distinct features of transverse bending moments are two “Kinks” with the same values in response. The RAOs of transverse bending moments in the bow quartering seas are presented in Fig. 26. In this case, transverse bending moments are nonlinear with respect to the wave frequencies and contain some “Kinks” for different speeds of the vessel. The peak magnitudes of the three speeds of the vessel are approximately the same.

The transverse bending moment's response in the head seas is depicted in Fig. 27. The responses are nonlinear throughout the frequencies and they also contain fewer “Kinks”. Different vessel speeds affect the peak magnitude. While the vessel speed of 30 knots has the highest response. The “Kinks” in the responses are due to the coupling of the transverse bending moment responses with the roll motions.

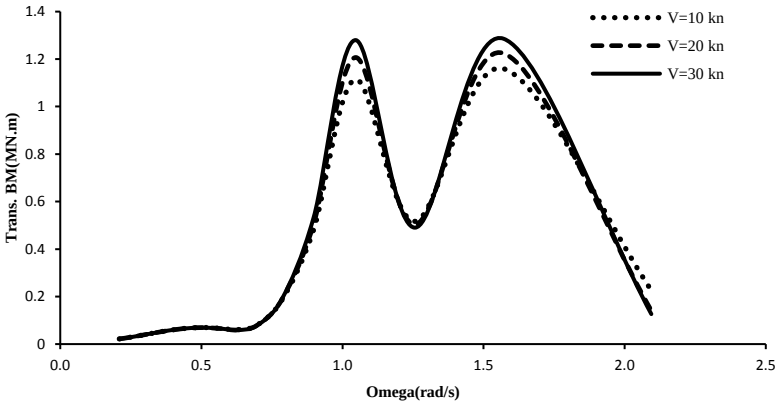

Fig. 25. RAOs of transverse bending moments at beam seas.

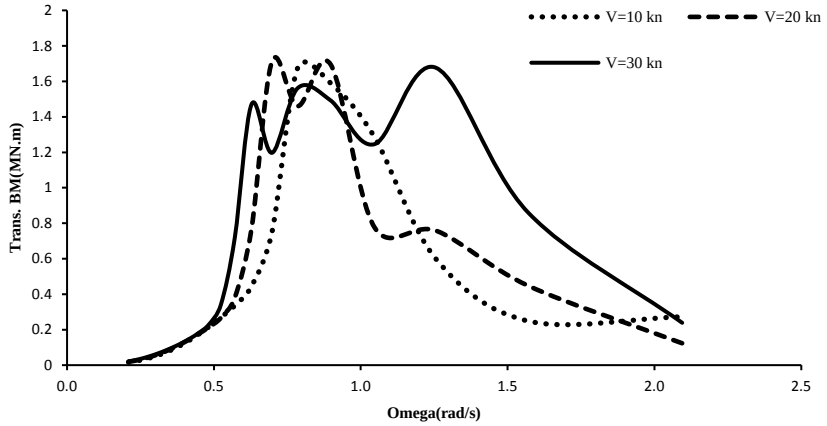

Fig. 26. RAOs of transverse bending moments at bow quartering seas.

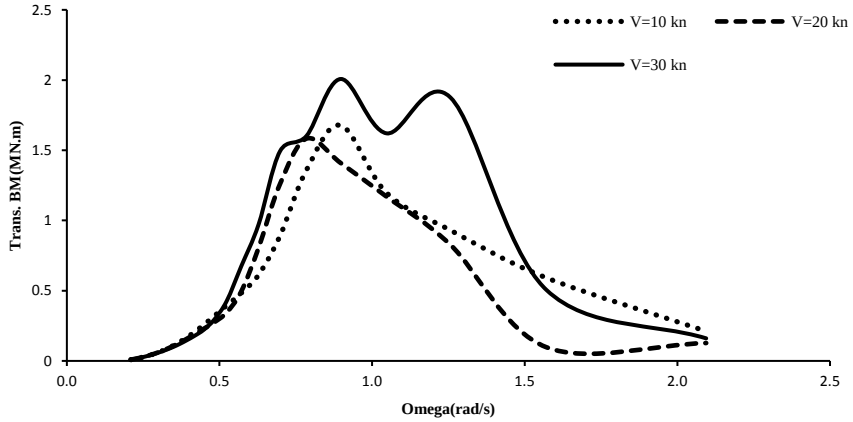

Fig. 27. RAOs of transverse bending moments at head seas.

The RAOs of transverse torsion moments are presented in Figs. 28 to 30. As shown in Fig. 28 the plots are similar in physical trends and the magnitudes of the responses to peak points increase with an increase in the vessel speed. The RAOs of transverse torsion moments in the bow quartering seas are presented in Fig. 29. In this case, transverse torsion moments are nonlinear with respect to the wave frequencies and contain some "Kinks" for different speeds of the vessel.

The "Kinks" in the forward speed is due to the coupling of the transverse torsion moment responses with the pitch motions. The response has the highest peak value at a vessel speed of 30 knots. As shown in Fig. 30 the distinct features of transverse torsion moments in the head seas are two peak points at 10 and 30 knots. The response has the highest peak value at a vessel speed of 30 knots.

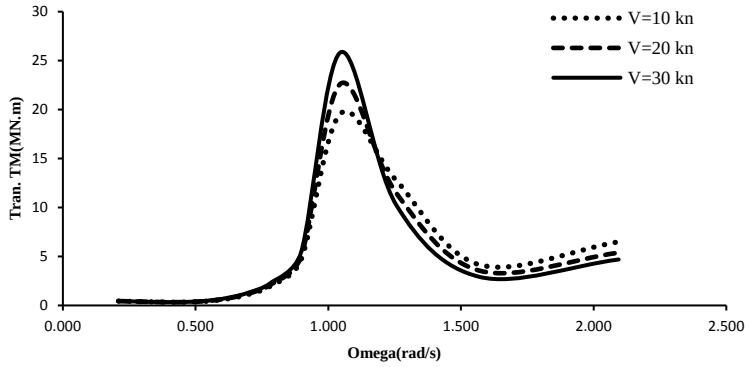

Fig. 28. RAOs of transverse torsion moments at beam seas.

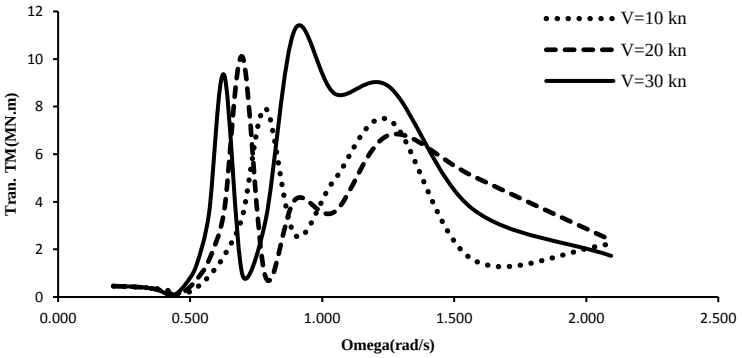

Fig. 29. RAOs of transverse torsion moments at bow quartering seas.

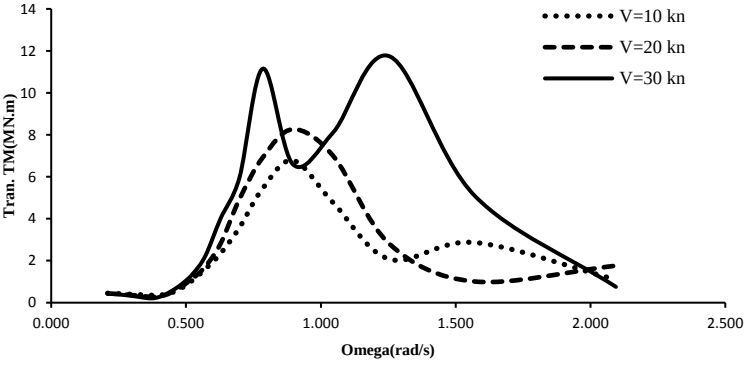

Fig. 30. RAOs of transverse torsion moments at head seas.

The RAOs of transverse shear forces are presented in Figs. 31 to 33. Figure 31 presents RAOs in beam seas. Responses are closely similar to transverse torsion moments in this heading. In the bow quartering and head seas as shown in Figs. 32

and 33, transverse shear forces are nonlinear with respect to the wave frequencies and contain some "Kinks" for different speeds of the vessel. These "Kinks" are due to the coupling of the roll motions with the responses of the transverse shear force. The response has the highest peak value at a vessel speed of 30 knots.

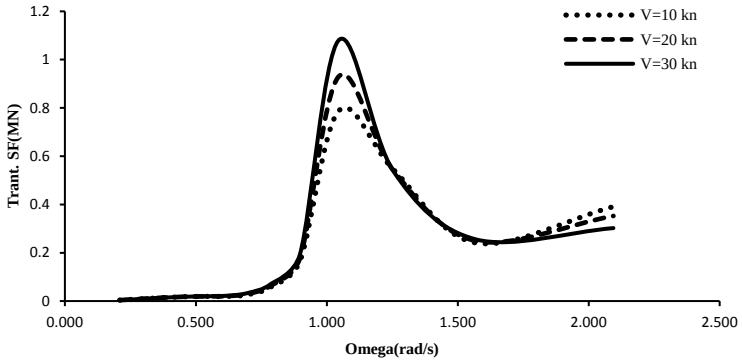

Fig. 31. RAOs of transverse shear forces at beam seas.

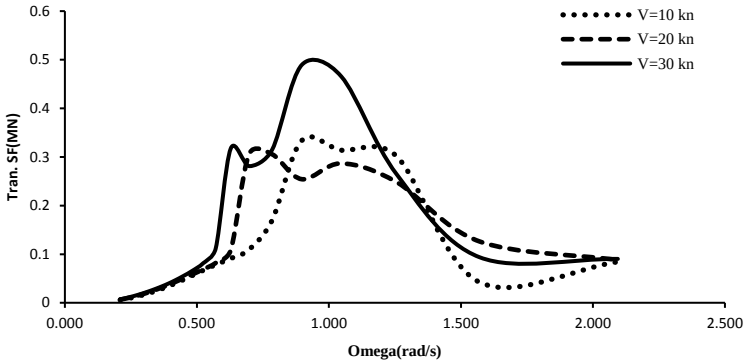

Fig. 32. RAOs of transverse shear forces at bow quartering seas.

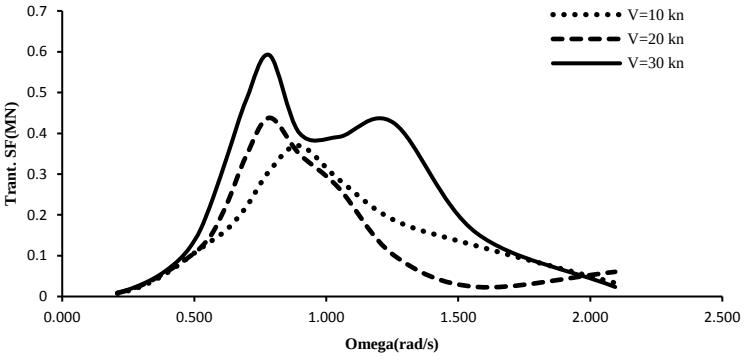

Fig. 33. RAOs of transverse shear forces at Head seas.

6. Conclusions

In this study, wave-induced motion and loads of trimaran ship at various forward speeds and wave headings have been conducted using a 3D panel method code, MAESTRO-Wave. In light of the results of the study, the most important conclusions are drawn as follows:

- The interactions between the motions with the wave-induced loads and individual motion responses together leads to the frequent appearance of "Kinks" in a coupled form with the responses of other motions or wave-induced loads. These couplings were observed mostly at higher frequencies and hurt the performance of the vessel. Such "Kinks" are also attributed to the effects of vessel speed changes since their magnitudes usually increase when the vessel speed increases.
- The trend of heave and pitch motion responses in head seas is similar to the bow quartering seas but with greater "Kinks" magnitudes. The peak magnitude of vertical bending moments is approximately the same in all the three different speeds for beam seas and bow quartering seas. Furthermore, maximum vertical bending moments and shear forces occur in sections of the main hull where side hulls are located.
- The motion and the wave-induced load responses in the beams seas were found to be less sensitive to the effects of the changes in the vessel speeds.
- In general, wave loads and speeds appear to be highly related in head seas, i.e. high speeds cause high wave loads, but their correlations are not obvious in beam and bow quartering waves.

Nomenclatures

A_{jk}	Matrix of added mass
A_{jk}	Matrix of added mass
B_{jk}	Matrix of the damping coefficient
C_{jk}	Matrix of restoring forces and Moments coefficient
M_j	Wave-induced bending moment
M_{jk}	Mass matrix
Q_j	Wave-induced shear force
X_j	Exciting forces and moments
U	Vessel speed

Greek Symbols

α	Wave amplitude
β	Relative wave heading
η_k	Body motions
ϕ_D	Diffraction potential
ϕ_I	Incident wave potential
ϕ_i	Radiation potential
$\phi(x,y,z)$	Total velocity potential
$\varphi(x,y,z)$	Disturbance potential
ω_e	Wave encounter frequency

References

1. Junwu, Z. (1997). *Design and hydrodynamic performance of trimaran displacement ships*. Ph.d. Thesis. Department of Mechanical Engineering University College London.
2. Fang, M.C.; and Chen, T.Y. (2008). A parametric study of wave loads on trimaran ships traveling in waves. *Journal of Ocean Engineering*, 35, 749-762.
3. Fang, M.C.; and Too, G.Y. (2006). The effect of side hull arrangements on the motions of the trimaran ship in waves. *Journal of Naval Engineering*, 118, 27-37.
4. Armstrong, T. (2006). On the performance of a large high-speed trimaran. *Australian Journal of Mechanical Engineering*, 3, 123-131.
5. Sato, Y.; Orihara, H.; and Miyata, H. (2006). Practical Application of two CFD codes for ship motions in arbitrary waves validation of motion prediction method for trimaran vessels. *Proceedings of the 26th Symposium on Naval Hydrodynamics*. Rome, Italy, 17-22.
6. Sato, Y.; Uzawa, K.; and Miyata, H. (2007). Validation of the motion prediction method for trimaran vessels. *Proceedings of the 9th International Conference on Numerical Ship Hydrodynamics (ICNSH)*. Michigan, USA.
7. Hebblewhite, K.; Sahoo, P.K.; and Doctors, L.J. (2007). Theoretical and experimental analysis of motion characteristics of a trimaran hull form. *Ships and Offshore Structures*, 2, 149-156.
8. Min, X.; and Shi-lian, Z. (2011). A numerical study on side hull optimization for trimaran. *Journal of Hydrodynamics*, 3, 265-272.
9. Mohammadi, M.; Khedmati, M.R.; and Vakilabadi, K.A. (2013). Effects of hull damage on global loads acting on a trimaran ship. *Journal of Ships and Offshore Structures*, 10, 635-652.
10. Vakilabadi, K.A.; Khedmati, M.R.; and Seif, M.S. (2014). Experimental study on heave and pitch motion of a wave-piercing trimaran. *Journal of Transactions of Faculty of Mechanical Engineering and Naval Architecture (FAMENA)*, 38, 13-26.
11. Pei, Z.; Zhu, Z.; and Wu, W. (2015). Research of load and structural direct calculation on flat-type river-sea-going ship, *Journal of Traffic and Transportation Engineering*, 3, 266-276.
12. Khoob, A.A.; and Ketabdari, M.J. (2017). A numerical investigation into the effects of long-term wave-induced loads on the cross structure of a wave-piercing trimaran, *Cogent Engineering*, 4, 1387951.
13. Adenya, C.; Ren, H.; and Qing, C. (2015). Numerical analysis of the motion and load responses of a 400,000 DWT ore carrier in waves. *Proceedings of OCEANS – Marine Technology Society (MTS)/Institute of Electrical and Electronics Engineers (IEEE)*. Washington, USA, 1-7.
14. Prini, F.; Benson, S.; Birmingham, R.W.; Sheppard, P.J.; Phillips, H.J.; and Mediavilla-Varas, J. (2015). Seakeeping analysis of a high-speed search and rescue craft by linear potential theory. *Proceedings of the International Conference on Lightweight Design of Marine Structures (LIMAS)*. Glasgow, UK, 87-96.
15. Xiaobo, W.; Ren, H.; Sun, Y.; Wang, D.; and Wang, Z.Y. (2016). Experimental investigation of wave loads based on trimaran self-propulsion

model. *Proceedings of the 35th International Conference on Ocean, Offshore and Arctic Engineering* (*OMAE*). Busan, South Korea, 7.

16. Jiao, J.; Sun, S.; and Ren, H. (2016). Predictions of wave-induced ship motions and load by large-scaled model measurement at sea and numerical analysis. *Journal of Brodogradnja/Shipbuilding*, 67(2), 81-100.
17. Khoob, A.A.; and Ketabdari, M.J. (2019). Wave-induced loads on cross-deck of a wave-piercing trimaran with different hull forms of outriggers. *Transport*, 34(5), 559-568.
18. American Bureau of Shipping. (2007). *Guide for building and classing high-speed naval craft: Part 3 (hull construction and equipment).* Houston (TX): American Bureau of Shipping.
19. Yan, L.; and Alan, B. (2012). *High Performance Marine Vessels*. New York: Springer
20. MAESTRO Version 10.0 Users' Manual. Stevensville (MD): Advanced Marine Technology Centre. From: http://www.maestromarine.com
21. ITTC Loads and responses seakeeping, verification and validation of linear and weakly nonlinear seakeeping computer code, Procedure 7.5-02-07-05 Rev 1 (2010).
22. Papanikolaou, A.D.; and Schellin, T.E. (2011). A three dimensional panel method for motions and loads of ships with forward speed. *Journal of Ship Technology Research*, 39, 147-156.